# Structural studies unravel the active conformation of apo RORγt nuclear receptor and a common inverse agonism of two diverse classes of RORγt inhibitors

Xiang Li[‡1], Marie Anderson[‡], Delphine Collin[‡], Ingo Muegge[‡], John Wan[‡], Debra Brennan[‡], Stanley Kugler[‡], Donna Terenzio[‡], Charles Kennedy[‡], Siqi Lin[‡], Mark E. Labadia[§], Brian Cook[‡], Robert Hughes[‡], and Neil A. Farrow[‡]

*From the Departments of [‡]Small Molecule Discovery Research and [§]Immunology and Respiratory Diseases, Boehringer Ingelheim Pharmaceuticals, Inc., Ridgefield, Connecticut 06877-0368*

Edited by Wolfgang Peti

The nuclear receptor retinoid acid receptor-related receptor γt (RORγt) is a master regulator of the Th17/IL-17 pathway that plays crucial roles in the pathogenesis of autoimmunity. RORγt has recently emerged as a highly promising target for treatment of a number of autoimmune diseases. Through high-throughput screening, we previously identified several classes of inverse agonists for RORγt. Here, we report the crystal structures for the ligand-binding domain of RORγt in both apo and ligand-bound states. We show that apo RORγt adopts an active conformation capable of recruiting coactivator peptides and present a detailed analysis of the structural determinants that stabilize helix 12 (H12) of RORγt in the active state in the absence of a ligand. The structures of ligand-bound RORγt reveal that binding of the inverse agonists disrupts critical interactions that stabilize H12. This destabilizing effect is supported by *ab initio* calculations and experimentally by a normalized crystallographic B-factor analysis. Of note, the H12 destabilization in the active state shifts the conformational equilibrium of RORγt toward an inactive state, which underlies the molecular mechanism of action for the inverse agonists reported here. Our findings highlight that nuclear receptor structure and function are dictated by a dynamic conformational equilibrium and that subtle changes in ligand structures can shift this equilibrium in opposite directions, leading to a functional switch from agonists to inverse agonists.

The Th17 lineage of T helper cells plays an essential role in protective immunity against a variety of bacteria such as *Mycobacteria tuberculosis* and *Staphylococcus aureus* and pathogenic fungi such as *Candida albicans* (1). Individuals with genetic defects in the Th17 pathway are susceptible to recurrent bacterial infections and often develop unrelenting chronic mucocutaneous candidiasis (2, 3). However, Th17 cells, which produce the eponymous IL-17A (often simply referred to as IL-17) and other proinflammatory cytokines, including IL-17F, IL-21, IL-22, and granulocyte-macrophage colony-stimulating factor (GM-CSF), are also potent inducers of multiple autoimmune diseases in animal models (4–8) and are strongly implicated by human genetic studies in the pathogenesis of most common human autoimmune diseases, including psoriasis, psoriatic arthritis, Crohn's disease, ankylosing spondylitis, rheumatoid arthritis, and multiple sclerosis (9–13). Given the prominent roles of the Th17/IL-17 pathway in autoimmunity, therapeutic interventions targeting this pathway have been intensely pursued. Two monoclonal antibodies (mAb) targeting IL-17A, secukinumab (Cosentyx) and ixekizumab (Taltz), have been approved recently for the treatment of moderate to severe plaque psoriasis. Secukinumab is also approved for psoriatic arthritis and ankylosing spondylitis (14). In phase 3 clinical trials, both secukinumab and ixekizumab have demonstrated remarkable efficacy for treatment of psoriasis with ∼90% of patients achieving a 75% reduction in psoriasis area and severity index (PASI75) and ∼40% achieving a PASI100 response with complete clearing of skin lesions (15). Similar efficacy has been achieved by brodalumab (Siliq), a mAb targeting the IL-17 receptor IL-17RA, which was recently approved by the United States Food and Drug Administration to treat adults with moderate to severe plaque psoriasis (16). Other mAbs, such as guselkumab, tildrakizumab, risankizumab (BI 655066), and AMG 139, that target the p19 subunit of IL-23, a critical cytokine for pathogenic Th17 lineage commitment and expansion, also show excellent efficacy for psoriasis (15). Collectively, the success of these biologics has strongly validated clinically IL-17, IL-17R, and IL-23, all key players in the Th17 pathway, as valuable therapeutic targets for autoimmune diseases.

The nuclear receptor (NR)[2] retinoic acid receptor-related orphan receptor γt (RORγt) is a master transcription factor of Th17 cells, being both necessary and sufficient for IL-17 expres-

sion, and it is essential in promoting Th17 cell differentiation while suppressing the Th1 program (17, 18). RORγt is also required for the production of IL-17 from other cell types, including γδ T cells, invariant natural killer T cells, and group 3 innate lymphoid cells, and is necessary for Th17 cells to produce other proinflammatory cytokines such as IL-22, GM-CSF, and the IL-23R (19). Therefore, small-molecule modulators against RORγt are also a highly attractive therapeutic modality that has the potential for meaningful pharmacological differentiation from the specific anti-IL-17 or anti-IL-23 mAbs. Many small-molecule modulators of RORγt have been reported in the literature in recent years, and two compounds have reached phase 2 clinical trials for treatment of psoriasis (20–22).

There are three members in the ROR subfamily of human NRs as follows: RORα (RORA, NR1F1), RORβ (RORB, NR1F2), and RORγ (RORC, NR1F3). The members of the subfamily share about 50% sequence identity in their ligand-binding domains (LBD). Two isoforms of RORγ exist: the canonical RORγ (RORγ1) and RORγt (RORγ2), which lacks the first 21 N-terminal amino acids due to alternative promoter usage. The RORγ isoform is expressed in most tissues and is involved in many physiological functions (23). In contrast, RORγt is solely expressed in lymphoid lineage cells of the immune system, consistent with its essential role in the development of lymph nodes as well as Th17 cells (23). Despite the word "orphan" in RORγ's name, recent studies with sterol auxotroph cells have convincingly shown that sterol lipids, including certain cholesterol biosynthetic intermediates and oxysterols, are physiological ligands for RORγ (24–26). An important link between lipid metabolism and regulation of Th17 pathogenicity was established recently by the discovery that CD5 antigen-like (CD5L) acts as a negative regulator that alters the balance of lipid saturation and directly affects the availability of sterol ligands for RORγt (27).

Crystal structures of RORγ LBD in complex with hydroxycholesterols and various synthetic ligands have been reported (28–36). But to our knowledge, no apo structure of RORγ LBD has yet been published. Here, we report the crystal structures of RORγt LBD in both apo and ligand-bound states with two novel classes of synthetic ligands. The apo RORγt structure adopts a predominantly active conformation, which is supported by the NMR experiments in solution. Density functional theory (DFT) calculations were used to elucidate the energetics of the structural determinants underlying the active conformation of RORγt. A common theme for the structural mechanism of action of the two distinct classes of inverse agonists was revealed from analyses of the respective complex structures and normalized crystallographic B-factors. We emphasize that the dynamic conformational equilibrium is a fundamental attribute to understand NR structure and function. Indeed, subtle changes in ligand structures can shift the equilibrium in opposite directions and lead to a functional switch from an agonist to an inverse agonist.

## Results

### Production and crystallization of SRC2 peptide-tethered RORγt-LBD

Structural studies of NRs are often carried out in the presence of carefully chosen cofactor peptides that bind and stabilize the receptors, as is the case in the first crystallographic study of the RORγt-LBD (28). When examining the published crystal structure (PDB code 3L0L), we noticed that the Cα–Cα distance is only 8 Å between the first resolved N-terminal residue of the steroid receptor coactivator-2 (SRC2) peptide and the C-terminal residue (Ser-507) of the RORγt-LBD. Modeling suggested that it might be possible to covalently tether an SRC2 peptide to the C terminus of RORγt-LBD via a simple -GGG- linker. The tri-glycine linker provides the maximal conformational flexibility to preserve the native interactions between the tethered partners with minimal interference. The tethered system is thermodynamically more stable than the untethered complex due to the reduction of macroscopic translational entropy through tethering (37, 38). We therefore produced the His$_6$-RORγt-LBD(260–507) -GGG- EKHKILHRLLQDS (SRC2 peptide) construct and expressed it in *Escherichia coli*. The chimeric protein expressed well in a soluble form and was straightforward to purify using standard affinity and size-exclusion chromatography (see under "Experimental procedures"). Similar approaches have been used in the study of the PXR-LBD–SRC-1p complex (39), as well as MHC-II–peptide complexes and other protein–protein interactions (40, 41). Without the complication of achieving the right stoichiometry for the peptide/receptor mixture, the apo crystals of RORγt-LBD with tethered SRC2 peptide could be reproducibly obtained by sitting or hanging drop vapor diffusion at room temperature (see under "Experimental procedures"). In most cases, co-structures with ligands were obtained by soaking of compounds into the apo RORγt-LBD crystals. Very occasionally, co-crystallization, where a compound was pre-incubated with the protein solution prior to crystallization, was also used to solve a co-complex structure. This is the case for compound **2** (Table 2), for which co-structures were obtained through both soaking and co-crystallization.

### Apo RORγt-LBD structure and the structural determinants for its active conformation

The apo RORγt-LBD structure was solved in the space group P4$_1$2$_1$2 with one polypeptide chain per asymmetric unit. The statistics for data collection and refinement are summarized in Table 1. The apo RORγt-LBD structure is very similar to that of the 25-hydroxycholesterol (25-HC)-bound RORγt (28) (PDB code 3L0L), with r.m.s.d. of backbone and all heavy atoms at 0.54 and 1.20 Å between the two structures, respectively (Fig. 1). Similar to 25-HC-bound RORγt, the apo structure assumes an active conformation, with H12 as an integral part of the AF-2 surface that captures the SRC2 coactivator peptide (Fig. 1A). The -GGG- linker residues are in a flexible loop conformation with weak electron densities and elevated B-factor values. There are no specific interactions between the glycine linker and the rest of the protein. Notably, the apo RORγt contains a large ligand-binding pocket, with a cavity volume of 940 Å$^3$ (Fig. 1A). As is typical for nuclear receptors, the ligand-binding pocket is predominantly hydrophobic (575 Å$^3$, 61% of total cavity volume). In contrast, the cavity volumes for hydrophilic, basic, and acidic compositions are 161 Å$^3$ (17%), 178 Å$^3$ (19%), and 26 Å$^3$ (3%), respectively. Interestingly, almost the entire 25-HC can fit comfortably in the ligand-binding pocket of apo

## Apo and ligand-bound RORγt structures

**Table 1**

**Data collection and structure refinement statistics**

Values in parentheses are for the last resolution shell. r.m.s.d. is root mean square deviation.

| RORγt LBD | Apo | With compound 1 | With compound 2 | With compound 3 |
|---|---|---|---|---|
| **Data collection** | | | | |
| Wavelength (Å) | 1.00 | 1.00 | 1.00 | 1.00 |
| Space group | P4₁2₁2 | P4₁2₁2 | P4₁2₁2 | P4₁2₁2 |
| Unit cell dimensions (*a*, *b*, *c*) (Å) | 61.27, 61.27, 154.23 | 62.31, 62.31, 154.18 | 60.47, 60.47, 155.00 | 62.96, 62.96, 155.32 |
| (*α*, *β*, *γ*) (°) | 90.00, 90.00, 90.00 | 90.00, 90.00, 90.00 | 90.00, 90.00, 90.00 | 90.00, 90.00, 90.00 |
| Mosaicity | 0.31 | 0.19 | 0.58 | 0.48 |
| Resolution range (Å) | 43.33–1.95 (2.02–1.95) | 77.09–2.04 (2.05–2.04) | 155.00–2.23 (2.233–2.226) | 77.66–2.34 (2.342–2.335) |
| Total no. of reflections | 258,813 | 261,150 | 182,584 | 175,314 |
| No. of unique reflections | 21,942 | 20,213 | 14,904 | 14,031 |
| Average redundancy | 11.80 (12.56) | 12.9 (12.6) | 12.3 (11.9) | 12.5 (13.3) |
| Completeness (%) | 98.5 (98.0) | 100.0 (100.0) | 100.0 (100.0) | 100.0 (100.0) |
| $R_{merge}$ | 0.074 (0.593) | 0.086 (1.202) | 0.099 (1.490) | 0.114 (1.903) |
| $R_{meas}$ | 0.078 (0.618) | 0.090 (1.254) | 0.104 (1.558) | 0.119 (1.978) |
| Output $\langle I/\sigma_I \rangle$ | 14.4 (3.2) | 25.0 (2.2) | 15.4 (2.4) | 18.9 (2.4) |
| **Refinement** | | | | |
| Resolution range (Å) | 43.33–1.95 | 39.65–2.04 | 39.28–2.23 | 38.62–2.34 |
| Reflections, work/test (%) | 21,934/1123 (5.12%) | 20,131/1002 (4.98%) | 14,824/739 (4.99%) | 13,954/704 (5.05%) |
| Completeness for range (%) | 98.82 | 99.95 | 99.85 | 99.89 |
| No. of atoms | 2300 | 2346 | 2268 | 2215 |
| No. of waters | 159 | 190 | 102 | 80 |
| $R_{work}$ | 0.1957 | 0.1866 | 0.1932 | 0.1836 |
| $R_{free}$ | 0.2298 | 0.2075 | 0.2344 | 0.2161 |
| r.m.s.d. bond lengths (Å) | 0.004 | 0.003 | 0.002 | 0.005 |
| r.m.s.d. bond angles (°) | 0.731 | 0.621 | 0.534 | 0.600 |
| Average B value (Å²) | 36.62 | 33.79 | 45.54 | 42.07 |
| **Ramachandran plot** | | | | |
| Favored (%) | 98.85 | 97.72 | 98.85 | 98.45 |
| Allowed (%) | 1.15 | 2.28 | 1.15 | 1.55 |
| Outliers (%) | 0.0 | 0.00 | 0.00 | 0.00 |

RORγt; only some adaptive side-chain movements from His-323, Leu-324, and Mer-365 are required to accommodate the B-ring of 25-HC (Fig. 1*B*). In fact, the His-323 side-chain conformation switch constitutes the largest structural difference between the apo and 25-HC bound RORγt. It has been shown recently that a number of cholesterol precursors, such as lanosterol and desmosterol as well as oxysterols, are the natural endogenous ligands for RORγt (24–26). Our structure of apo RORγt suggests that the ligand-binding pocket may be preformed to readily accommodate such ligands.

The question then arises as to how RORγt keeps H12 in the active conformation and maintains a large cavity in its interior in the absence of a ligand. One key structural element is the His-479–Tyr-502–Phe-506 triplet. Tyr-502 and Phe-506 reside on the same face of the two-turn H12, forming close interactions with His-479 on H11 (Fig. 1*C*). The most prominent of the interactions is the H-bond between the phenol of Tyr-502 and the imidazole $N^{\epsilon 2}$ of His-479. Here, the $N^{\epsilon 2}$ of His-479 acts most likely as an H-bond acceptor, and thus His-479 is in the neutral (uncharged) form. His-479 also engages in an edge-to-face aromatic packing interaction with Phe-506. Furthermore, a favorable aromatic ring packing exists between Tyr-502 and Phe-506. The side-chain rotamer of His-479 is further stabilized through a water-mediated H-bond network linking its $N^{\delta 1}$ to the backbone carbonyl oxygen of Gln-475. To more quantitatively assess the significance of these interactions, an *ab initio* calculation of the interaction energy among the side chains of the HYF triplet was carried out using the DFT method (see under "Experimental procedures"). The DFT calculation used the Truhlar hybrid meta exchange-correlation functional M06-2X with a 6–32G** basis set, which is well-suited for calculating non-covalent interactions such as

H-bonding and π-stacking that are dominated by dispersion forces (42, 43). The resulting interaction energy for the HYF triplet is −12.90 kcal/mol. This is a very significant energy that provides the anchoring force to stabilize H12 of RORγt in the active conformation in the absence of a ligand. The HYF triplet is conserved among the α/β/γ isoforms of the ROR subfamily but is not found in any other NRs. For example, the corresponding residues in PPARγ are His-449–Leu-469–Tyr-473 with no H-bonding among them. The interaction energy is only −3.00 kcal/mol when PPARγ is in the active conformation and is negligible when PPARγ is in the inactive conformation (interaction energies calculated using the same DFT method, with PPARγ coordinates from PDB code 1PRG) (see supplemental Fig. S1). Because of the lack of a stabilizing triplet in PPARγ, H12 and indeed the entire ligand-binding pocket of apo PPARγ exhibit significant conformational mobility as revealed by NMR (44) and fluorescence anisotropy studies (45). The crystal structure of apo PPARγ also showed elevated crystallographic B-factor values for the H12 and ligand-binding pocket residues, and H12 was in fact captured in both active and inactive states (46).

There is another unique structural element in ROR, namely the H11′ helix. Again, H11′ is present in all three isoforms of the ROR subfamily but is not found in most of the other NRs. As illustrated in Fig. 1*D*, H11′ and H12 together bury 322 Å² of solvent-accessible surface area, which is 29% of H12's total surface area. Therefore, a notable helical packing interaction exists between H11′ and H12. Helical packing in general is an important stabilizing force in protein folding and in protein-protein interactions (47, 48). Here, the H11′–H12 packing contributes to stabilize H12 in the active conformation. Interestingly, H12 and the SRC2 peptide together bury 509 Å² of solvent-accessible surface area (Fig. 1*D*), which amounts to 46% and 32% of
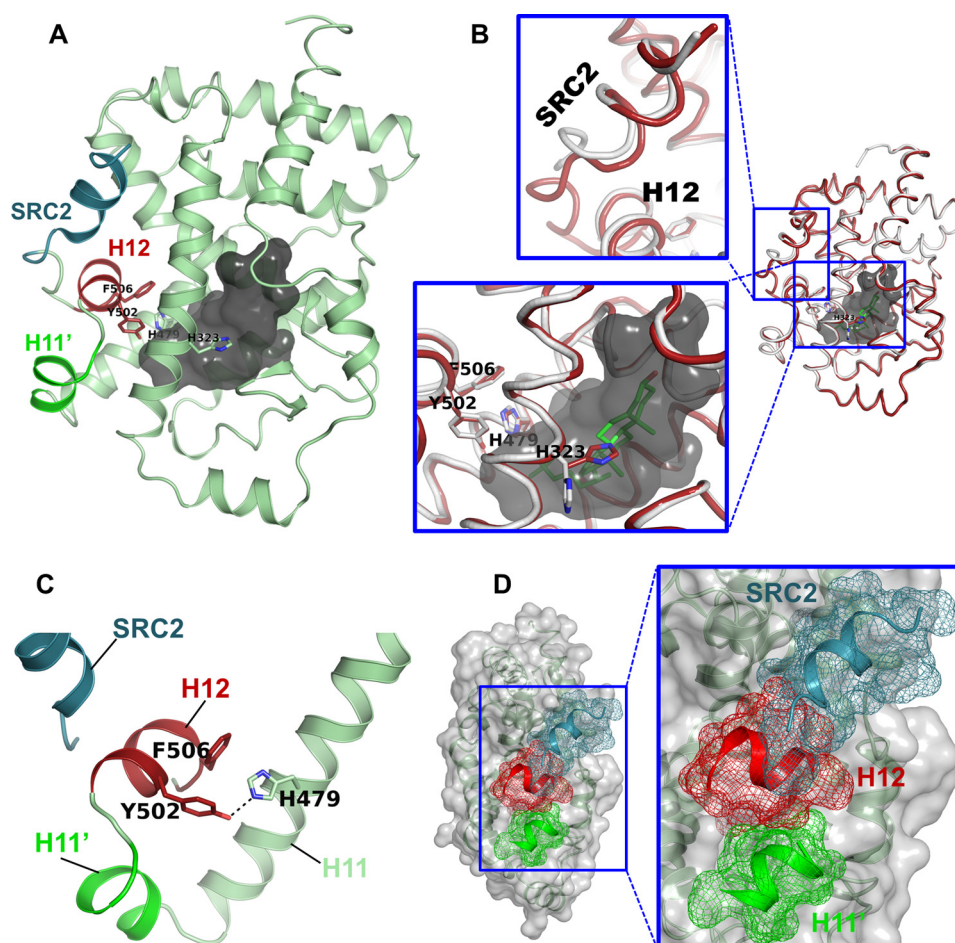
**Figure 1. Apo structure of RORγt LBD and structural determinants for its active conformation.** *A,* schematic representation of the apo RORγt LBD is shown in *pale green,* with H11′, H12, and SRC2 peptide segments highlighted in *green, dark red,* and *xenon blue,* respectively. The large cavity present in the apo RORγt is shown in *dark gray.* His-323, His-479, Tyr-502, and Phe-506 are highlighted as *sticks. B,* superposition of the apo RORγt structure in *dark red* with the RORγt LBD bound with 25-HC in *light gray* (PDB code 3L0L); 25-HC is drawn as *green sticks.* Close-up views are shown for the SRC2 peptide and H12 regions and for the apo state cavity with 25-HC and His-323, His-479, Tyr-502, and Phe-506 highlighted. The B-ring of 25-HC protrudes out of the apo cavity and would clash with the side chain of His-323 in the apo state. *C,* close interactions among the His-479–Tyr-502–Phe-506 triplet in RORγt help to anchor helix 12 in the active conformation. Color scheme follows that of *A.* The H-bond between His-479 and Tyr-502 is indicated as *black dashes. D,* helical packing between H11′, H12 and the SRC2 peptide provides further stabilization. The solvent-accessible surface areas of the three helical elements are depicted as *meshes* and highlighted in a close-up view. Color scheme follows that of *A.*

total surface area for H12 and the SRC2 peptide, respectively, and it underscores the critical role H12 plays in recruiting coactivators. In summary, RORγt utilizes a unique HYF triplet to provide significant interaction energy to anchor H12 in the active conformation, which is further stabilized by helical packing with a unique H11′ element.

### RORγt-LBD is capable of recruiting coactivator peptide in the absence of a ligand

A hallmark of NR in the active state is its ability to recruit coactivators to initiate transcription. To investigate whether apo RORγt is competent to bind coactivators, we carried out solution NMR studies using $^{13}$C/$^{15}$N-labeled samples from a RORγt(259–518) construct as well as the crystallography construct RORγt(260–507)-G$_3$-SRC2. The RORγt(259–518) construct encompasses the entire RORγt ligand-binding domain, without C-terminal truncation beyond H12 and without tethering of a coactivator peptide. As shown in Fig. 2, titration of the SRC2 peptide into the $^{13}$C/$^{15}$N-labeled RORγt(259–518) protein resulted in distinctive chemical shift perturbations to the

backbone amide peaks in the $^{15}$N-TROSY spectra (Fig. 2A) as well as to the methyl peaks in the $^{13}$C-HSQC spectra (Fig. 2B) of RORγt(259–518). These results clearly demonstrate that the native RORγt-LBD in solution is capable of binding to a coactivator peptide, such as the SRC2 peptide used here, in the absence of a ligand. Furthermore, the backbone $^{15}$N-TROSY spectrum of the SRC2-bound RORγt(259–518) bears strong resemblance to that of the RORγt(260–507)-G$_3$-SRC2 (Fig. 2C). Some of the differences between the two spectra with proton chemical shifts centered around 8 ppm in Fig. 2C are likely due to the difference of C-terminal sequences after residue 507. The resemblance is even more striking for the methyl resonances in the $^{13}$C-HSQC spectra (Fig. 2D and compare with *B*), with the perturbed methyl peaks from RORγt(259–518) shifting to the exact positions of the corresponding methyl peaks from RORγt(260–507)-G$_3$-SRC2. Therefore, the SRC2-tethered RORγt-LBD largely recapitulates the native RORγt-LBD in the presence of the SRC2 peptide in solution. It should be noted from qualitative assessments of the NMR spectra that the native apo RORγt-LBD exhibits more conformational flexibil-
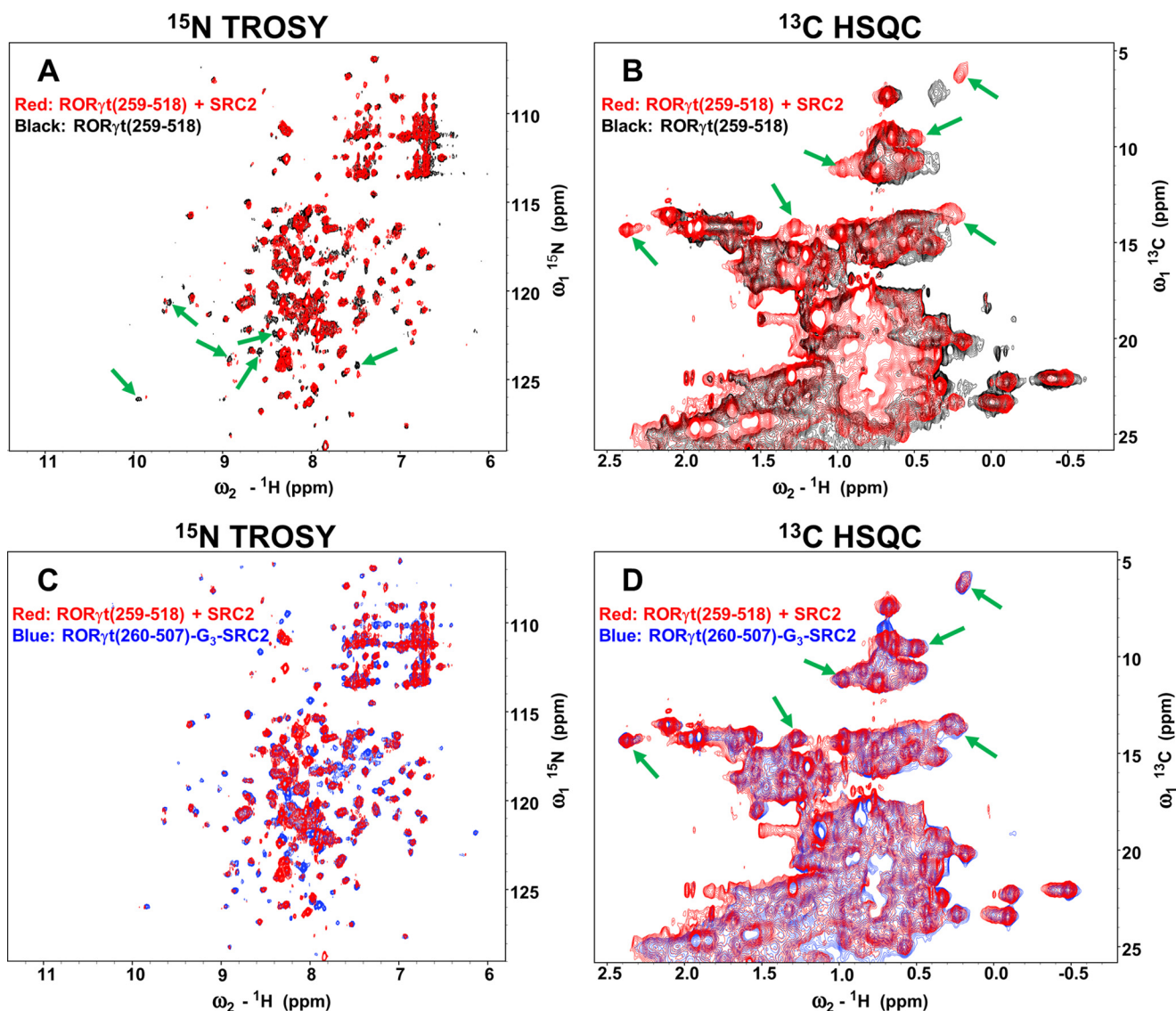
## ¹⁵N TROSY



## ¹³C HSQC



## ¹⁵N TROSY



## ¹³C HSQC



**Figure 2. NMR spectra of RORγt(259–518) and RORγt(260–507)-G₃-SRC2.** *A* and *B*, overlays of backbone ¹⁵N-TROSY (*A*) and methyl-¹³C-HSQC (*B*) spectra of RORγt(259–518) in apo (*black*) and in SRC2 peptide-bound state (*red*). Some perturbed peaks are highlighted with *green arrows*. *C* and *D*, overlays of backbone ¹⁵N-TROSY (*C*) and methyl-¹³C-HSQC (*D*) spectra of RORγt(260–507)-G₃-SRC2 (*blue*) and SRC2 peptide-bound RORγt(259–518) (*red*). The methyl peaks highlighted in Fig. 3*B* are indicated with the same *green arrows* in Fig. 3*D*.
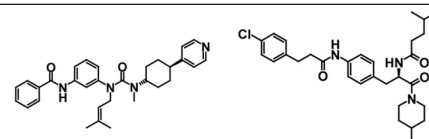
ity in solution than the SRC2-tethered apo RORγt-LBD. There is also evidence that the C-terminal residues beyond H12 (*i.e.* residues 508–518) in the native RORγt-LBD are largely disordered both in solution and in crystal forms.[3]

### Binding mode of two diverse classes of RORγt inverse agonists and the structural mechanism of action (sMOA)

Two classes of RORγt inverse agonists were discovered through a high-throughput screening campaign using a RORγt gene reporter assay (see under "Experimental procedures"). Two representative compounds from the two classes are shown in Table 2. These compounds had sub-micromolar binding affinity to RORγt in a fluorescence polarization (FP) competition assay using a probe with similar potency in a cell-based

**Table 2**

**Inverse agonists of RORγt reported in this study**



|  | **Compound 1** | **Compound 2** |
|---|---|---|
| RORγt Binding K$_d$ (µM) | 0.43 ± 0.18 | 0.35 ± 0.22 |
| RORγt RGA IC$_{50}$ (µM) | 0.64 ± 0.12 | 0.56 ± 0.15 |
| Th17 IC$_{50}$ (µM) | 0.9 ± 0.8 | 1.5 ± 0.6 |

RORγt reporter gene assay. More importantly, these compounds also demonstrated Th17 primary cell activity, inhibiting the production of IL-17.

A 2.04-Å resolution co-complex structure of compound **1** with RORγt-LBD was obtained through soaking of the com-

---

[3] Unpublished in-house NMR and X-ray data suggest that the C-terminal residues beyond H12 (*i.e.* residues 508–518) in the native RORγt-LBD are largely disordered both in solution and in crystal forms.
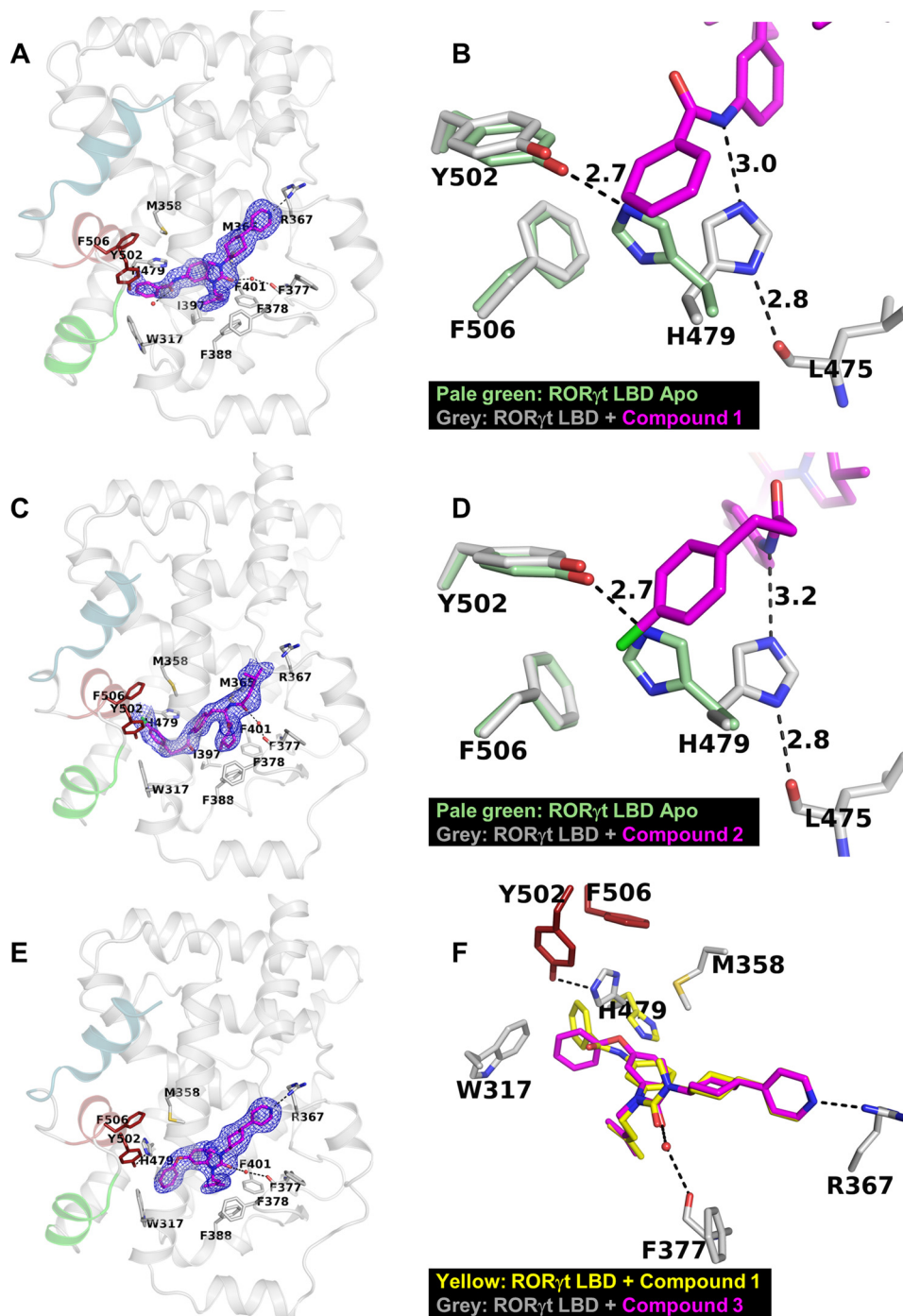
**Figure 3. Binding modes of compounds 1–3.** Compounds are shown in *magenta* in the ligand-binding pocket of RORγt of the respective co-complex structures. The overall structures of ligand-bound RORγt LBD are depicted as schematics, with H11′, H12, and SRC2 peptide colored as in Fig. 1A and key ligand-binding site residues highlighted as *sticks*. The simulated annealing omit difference maps were calculated with the entire compound molecules omitted and plotted in *blue* at 2.5 σ level for compounds **1** and **2** and at 3.0 σ level for compound **3**. The apo structure of RORγt is shown in *pale green* as in Fig. 1A. Compounds are shown as *magenta sticks*. H-bonds are indicated as *black dashes*. *A,* overall binding mode of compound **1**. *B,* close-up view of disruption of compound **1** to the His-479–Tyr-502–Phe-506 triplet in RORγt. *C,* overall binding mode of compound **2**. *D,* close-up view of disruption of compound **2** to the His-479–Tyr-502–Phe-506 triplet in RORγt. *E,* overall binding mode of compound **3**. *F,* cluster of aryl interactions are formed between compound **3**, the His-479–Tyr-502–Phe-506 triplet, and Trp-317, which further stabilize RORγt in the active conformation. Compound **1** and His-479 from compound **1**-bound RORγt are shown in *yellow* for comparison; only protein atoms were used in the superposition.

pound in the apo RORγt crystals. As shown in Fig. 3A, compound **1** binds across the entire cavity of the ligand-binding pocket, starting from one end with the pyridine nitrogen making a strong H-bond with Arg-367, the urea carbonyl in the middle forming a water-mediated H-bond with the backbone

carbonyl of Phe-377, and the isobutylene moiety extending into a highly hydrophobic region lined with aliphatic and aromatic residues, and ending with the phenyl amide interacting with the critical HYF triplet. Most notably, the phenyl ring of compound **1** protrudes into the His-479–Tyr-502 pair, disrupting the H-bond
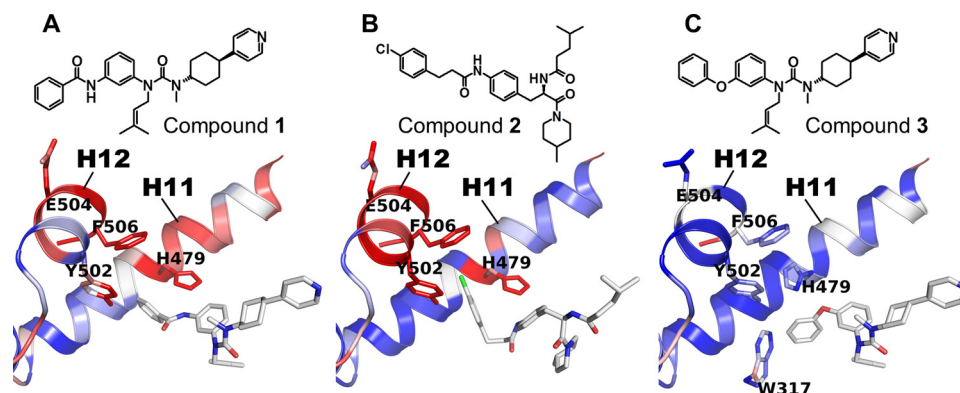
**Figure 4. Differential B-factor plot.** Normalized B-factor differences (see text) are displayed for the structural elements as a *blue-white-red* color ramp with *blue* indicating the most negative value (stabilization) and *red* the most positive value (destabilization). The compound chemical structure is drawn at the *top* of each respective panel. *A,* H11 and H12 of RORγt in complex with compound **1**. *B,* H11 and H12 of RORγt in complex with compound **2**. *C,* H11 and H12 of RORγt in complex with compound **3**.

between them. His-479 is forced to adopt a different side-chain conformation, which is stabilized through the formation of two new H-bonds with the amide linker of compound **1** and the backbone carbonyl of Leu-475, respectively (Fig. 3*B*). The two aromatic residues on H12, Tyr-502 and Phe-506, however, lose their close interactions with His-479. In this case, the interaction energy of the HYF triplet is reduced to only −1.4 kcal/mol as calculated using the same DFT protocol, which amounts to a loss of 11.5 kcal/mol stabilizing energy for H12 compared with the apo structure. Therefore, the disruption by compound **1** of the critical H-bond between His-479 and Tyr-502, with a concurrent loss of the aromatic packing between His-479 and Phe-506, results in the severe destabilization of H12 in its active conformation.

Compound **2** is structurally very different from compound **1**. To understand how compound **2** binds to RORγt and what is the structural basis for its mechanism of action, we also solved its co-complex structure with RORγt-LBD. Both soaking and co-crystallization approaches were attempted, and both yielded co-structures that were highly similar to each other; therefore, only the structure from co-crystallization is reported here. Despite having completely unrelated chemical structures, compounds **1** and **2** occupy essentially the same space in the ligand-binding pocket of RORγt (Fig. 3*C*). The isobutyl group of compound **2** aligns with the pyridyl ring of compound **1**, although the former does not engage Arg-367 in an H-bond. The methyl piperidine moiety of compound **2** fills the same hydrophobic sub-pocket that accepts the isobutylene moiety of compound **1**. A very similar water-mediated H-bond is observed between compound **2** and the backbone carbonyl of Phe-377. Most interestingly, the chlorobenzyl group of compound **2** also intercalates into the His-479 – Tyr-502 pair, forcing a side-chain conformation switch for His-479 and breaking up the His-479 – Tyr-502 H-bond (Fig. 3*D*). The interaction energy of the HYF triplet is lost almost completely at −1.1 kcal/mol based on the DFT calculation. The loss of favorable interactions for His-479 is partly compensated for by the formation of new H-bonds with the amide linker of compound **2** and the backbone carbonyl of Leu-475, in a way reminiscent of the case with compound **1**. Therefore, it appears that we have uncovered a common mechanism by which diverse chemical scaffolds may exert inverse agonist activities against RORγt through direct disruption

of the tightly interacting HYF triplet thereby destabilizing the active conformation of RORγt.

### Differential B-factor analysis

The crystallographic B-factor, also called atomic displacement parameter, is a measure of atomic displacement from its equilibrium or mean position, and it captures structural flexibility as well as positional variations due to thermal vibrations. Not surprisingly, B-factors have been widely exploited to probe protein flexibility (49), thermal stability (50), enzyme-active sites (51), and more recently to provide an integrated description of protein dynamics by combining with order parameters derived from solution NMR studies (52). Likewise, we reasoned that the destabilization of RORγt's H12 due to the binding of compounds **1** and **2** should be manifested by elevated B-factors in the H12 region of the respective complex structures. Typically, B-factor analyses of proteins are performed to compare different regions of the same protein structure. Here, we want to compare B-factors in the same regions of the protein from two different structures. To allow for a meaningful comparison of B-factors between the H12 region of interest in the bound state and the corresponding apo state, we first introduce a modified B-factor as shown in Equation 1,

$$B' = \frac{B - \langle B \rangle_{\text{median}}}{\langle B \rangle_{\text{median}}} \qquad \text{(Eq. 1)}$$

where $\langle B \rangle$ is the median B-factor, calculated separately for backbone and side-chain atoms, respectively. $B'$ can be viewed as a normalized B-factor. It is not influenced by variation of overall B-factors between different crystals. $B'$ is dimensionless. A negative (positive) $B'$ value can be interpreted as indicative of higher (lower) rigidity and stability than the average of the structure. To identify regions of altered flexibility or stability in the compound-bound complex *versus* the corresponding apo state, we examine Equation 2,

$$B_{\text{diff}} = B'_{\text{complex}} - B'_{\text{apo}} \qquad \text{(Eq. 2)}$$

An atom with positive $B_{\text{diff}}$ means it has elevated flexibility and is less stable compared with its apo state. Conversely, an atom with negative $B_{\text{diff}}$ means it is further rigidified and more stable than in
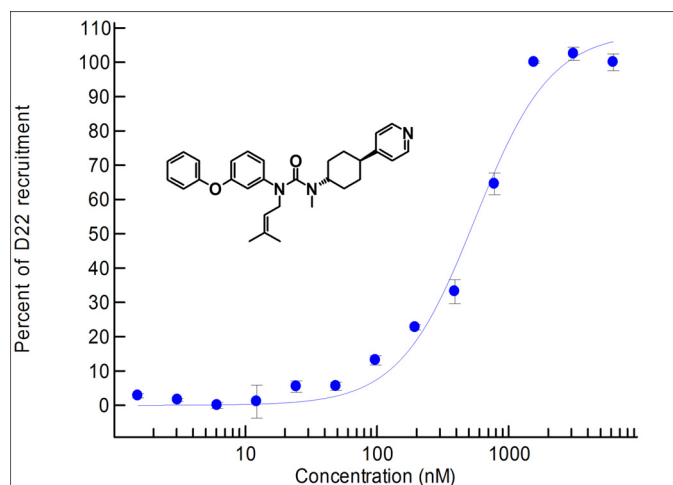
**Figure 5. Agonistic effect of compound 3 as shown in the FP-based coactivator recruitment assay.** The compound concentration is plotted in logarithmic scale.

the apo state. In Fig. 4, the $B_{diff}$ values are visualized with color ramps from blue (negative) to white (0) to red (positive) for H11 and H12 of RORγt in complex with compounds **1** (Fig. 4*A*) and **2** (Fig. 4*B*), respectively. As already suggested by the DFT calculations, the destabilization of H12 and the HYF triplet by the ligands is reflected in the $B_{diff}$ plots by red colorations of H12.

In addition to showing how ligands can destabilize H12, we surmised that it should also be possible that ligands can further stabilize H12 in the active conformation. To this end, we studied compound **3**, which was synthesized as an analog of compound **1** following a typical structure-activity relationship (SAR) optimization strategy. Compound **3** is structurally very similar to compound **1** except having an ether linker in place of an amide in compound **1**. Compound **3** showed good binding to RORγt (FP $K_d$ = 0.19 μM), but surprisingly it did not register an inhibitory activity in the reporter gene assay (IC$_{50}$ >3.3 μM). To understand its unexpected lack of inverse agonist activity, we solved a 2.34 Å resolution co-complex structure of compound **3** with RORγt-LBD through soaking of the compound in the apo RORγt crystals (Fig. 3*E*). Surprisingly, compound **3** does not disrupt the tightly interacting HYF triplet. Instead, the phenyl ether of compound **3** points toward Trp-317 and forms a tightly packed aromatic cluster with the HYF triplet and Trp-317 together, thereby further stabilizing RORγt in the active conformation (Fig. 3*F*). This stabilization effect is confirmed by the differential B-factor analysis shown in Fig. 4*C*. Because the inverse agonist activities of compound **1** and **2** are due to their destabilization effect on the active receptor conformation of RORγt as discussed above, it is expected that stabilization of the active conformation by compound **3** would elicit the opposite effect on the receptor. In other words, compound **3** should be an agonist of RORγt. A fluorescence polarization (FP)-based coactivator recruitment assay using a fluorescein-labeled coactivator peptide (D22) containing the L*XX*LL motif was developed to test this. As shown in Fig. 5, compound **3** indeed behaves as an agonist by enhancing the recruitment of D22 with an EC$_{50}$ of 0.54 μM.

## Discussion

Nuclear receptors are ligand-regulated transcription factors that orchestrate the assembly of coregulatory complexes (coactivators and corepressors) to modulate transcription through chromatin-remodeling activities (53). The role of a high affinity endogenous ligand is "classically" viewed as a trigger of a molecular switch whereby the binding of the ligand induces a conformational change involving H12 that switches the receptor from an inactive or repressed state to an active state competent for recruitment of coactivators and subsequent initiation of transcription (54). This conceptually appealing but overly simplistic view of NR activation is still frequently cited in the literature, even though mounting evidence has accumulated revealing NR proteins are highly dynamic and versatile. For instance, REV-ERBα (NR1D1) and REV-ERBβ (NR1D2) do not even have a H12 and use heme as a ligand (55, 56); NR activities are spatially and temporally regulated (57) and involve multiple structural elements with specific higher-order structures at play (58, 59). NRs are also known to be regulated by ligand-independent mechanisms such as post-translational modifications (60, 61). For example, RORγt has been shown to be modulated by both acetylation (62) and ubiquitination (63) with direct functional effects on Th17 biology. In this study, we showed that the apo RORγt LBD can adopt an active conformation with the capability to recruit a coactivator peptide. We believe that this active conformation is not influenced by the triple-glycine linker because these glycines do not make any specific contacts with the rest of the protein in the crystal structure and are highly flexible with very weak electron densities and high B-factors. In full support of this notion, our solution NMR studies with the RORγt(259–518) construct demonstrated that the non-tethered native RORγt LBD is capable of directly binding to the SRC2 coactivator peptide in the absence of a ligand, and the NMR spectra of SRC2-bound RORγt LBD closely resemble those of the SRC2-tethered RORγt-LBD, suggesting both having similar conformations in solution.

A number of NRs, such as estrogen-related receptor γ (ESRRG) (NR3B3), nerve growth factor IB (NGFIB) (NR4A1), nuclear receptor-related 1 (NURR1) (NR4A2), and liver receptor homolog-1 (LRH-1) (NR5A2), are capable of adopting active conformations independent of ligands (64). The crystal structure of apo LRH-1 (65) in particular shows an active conformation with a voluminous but empty cavity (820 Å) in the ligand-binding pocket, very similar to the case with apo RORγt revealed here. The specific structural elements stabilizing apo LRH-1 in the active conformation have been attributed to an extended H2 that acts as an extra layer with optimal helical packing against H3 to hold AF2 helices, including H12, in the activated state (65). In this study, we have carried out detailed structural and computational analyses to demonstrate that the tightly interacting His-479–Tyr-502–Phe-506 triplet is the primary structural element responsible for anchoring RORγt in the active conformation, which is further strengthened by additional helical packing with the extra H11′ helix. Both the HYF triplet and the H11′ are structural features unique to the ROR subfamily of NRs.

## Apo and ligand-bound RORγt structures

Proteins exist not in a single fixed state but rather as a dynamic ensemble in the biologically relevant environment. The apo crystal structure of RORγt LBD reported here is only a snapshot of a continuum of conformations sampled by RORγt in solution. The snapshot revealed by crystallography represents a low energy state having a dominant population. Under physiological conditions, RORγt should also be able to sample other lower population (higher energy) states, including inactive ones. In fact, our NMR studies with the RORγt(259−518) construct have confirmed that RORγt can indeed bind directly to a corepressor peptide derived from the silencing mediator of retinoid and thyroid hormone receptors-2 (SMRT2) in solution in the absence of a ligand (supplemental Fig. S2). Therefore, we have shown that RORγt has the conformational elasticity to bind either a coactivator (active conformation) or a corepressor (inactive conformation) in solution independent of ligands. It would be reasonable to posit that in general the presence of ligands or coregulators can alter the populations of various distinct states an NR may assume and shift the conformational equilibrium toward further activation or inactivation of the receptor. Under this dynamic equilibrium paradigm of NR modulation, the abundance of specific ligands, coactivators, or corepressors would dictate the activation state of an NR in a particular cellular context.

The sMOA revealed by the crystallographic studies of the two novel classes of RORγt inverse agonists dovetails with the dynamic equilibrium paradigm. Despite their high structural diversity, the two classes of inverse agonists share a common sMOA; they both disrupt the critical HYF triplet anchor thereby destabilizing the active conformation of H12 and shifting RORγt toward inactivation. Conversely, an agonist of RORγt should do the opposite. This is the case with compound **3**, which forms an extended aromatic cluster together with the HYF triplet and further stabilizes H12 in the active conformation. The dynamic picture of H12 mobility and stability in response to ligand binding is supported by the differential B-factor analysis as well as the *ab initio* calculations of the interaction energies employed in this study. Recently, cholesterol biosynthetic intermediates have been identified as natural ligands for RORγt. We believe that these endogenous ligands work similarly to compound **3** in that they also bind and further stabilize the active conformation of RORγt. Under physiological conditions, the actions of endogenous ligands are likely necessary to achieve sustained activation of RORγt due to other factors that can tilt the conformational equilibrium of the receptor toward repressed states.

Finally, it is interesting to note that subtle changes in the ligand structure can result in diametrically opposite functional responses of a nuclear receptor, as demonstrated by the two structurally very similar urea compounds **1** and **3** reported here. This phenomenon can be understood most naturally from examining the dynamic equilibrium of receptor states, as compounds **1** and **3** shift the conformational equilibrium of RORγt in opposite directions. Similar results have been reported by Rene *et al.* (35), who showed a class of benzylsulfonamides as full inverse agonists of RORγt with phenylsulfonamide analogs showing agonistic activities. The underlying sMOA described by the Genentech group is identical to what we have observed here, in that the phenylsulfonamides stabilize the active conformation of RORγt, and the benzylsulfonamides destabilize it. The subtleties that minimal variation of ligand structures can lead to dramatically different functional activities are not limited to NRs but are in fact well known in the GPCR field (66). Complex dynamic states are involved in the ligand regulation as well as signal transduction of GPCRs (67, 68). The dynamic equilibrium paradigm appears to be a unifying framework applicable for understanding the subtle structure-activity relationships often encountered in receptor drug discovery.

## Experimental procedures

### Cloning, expression, and purification

Constructs for His$_6$-Thr-RORγt(260−507)-GGG-SRC2 and His$_6$-Thr-RORγt(259−518) were cloned into pET41a(+) vectors. The proteins were expressed in *E. coli*, strain BL21(DE3). Cell cultures were grown in TB media under kanamycin control at 37 °C until the optical absorbance at 600 nm reached 1.0. Temperature was then reduced to 18 °C, and expression was induced with 0.5 mM isopropyl 1-thio-β-D-galactopyranoside. The $^{13}$C/$^{15}$N-labeled samples were expressed in $^{13}$C/$^{15}$N-enriched Bioexpress cell growth media (Cambridge Isotope Laboratories, Inc., catalogue no. CGM-1000-CN). Cells were lysed in lysis buffer (20 mM Tris, pH 8.0, 150 mM NaCl, 0.5% CHAPS, 2 mM β-mercaptoethanol, 10% glycerol, 2 tablets/50 ml protease inhibitors (Roche Applied Science catalogue no. 12483700), 10 units/ml benzonase nuclease (Sigma catalogue no. E1014), and 0.1 mg/ml lysozyme). After clarification by centrifugation at 4 °C, the soluble lysate was loaded onto a His-Trap column pre-equilibrated with Ni-Eq. buffer (20 mM Tris, pH 8.0, 150 mM NaCl, 2 mM β-mercaptoethanol, 10% glycerol, 0.05% CHAPS), and the protein was eluted out with elution buffer (20 mM Tris, pH 8.0, 150 mM NaCl, 2 mM β-mercaptoethanol, 10% glycerol, 0.05% CHAPS, and 500 mM imidazole). The eluted protein was further purified by size-exclusion chromatography on a Superdex 75 column. Finally, the pure RORγt protein was dialyzed into the storage buffer (25 mM HEPES, pH 7.0, 150 mM NaCl, 2 mM DTT) and concentrated to 9 mg/ml prior to crystallization. For NMR experiments, $^{13}$C/$^{15}$N-labeled protein samples were purified similarly and exchanged into the final NMR buffer (see below) and concentrated to 0.22 mM.

### Crystallization, data collection, and structure determination

Initial screens of crystallization conditions were carried out with Crystal Screens I and II from Hampton Research, and NR-LBD HT-96 screening kit from Molecular Dimensions (MD1–34), using sitting drop vapor diffusion on a Mosquito instrument at 20 °C. Drops containing 0.1 μl of protein mixed with 0.1 μl of well solution were equilibrated against 80 μl of well solution. Follow-up optimizations were performed manually using hanging drop vapor diffusion with drops containing 1 μl of protein mixed with 1 μl of well solution equilibrated against 500 μl of well solution. Diffraction-quality apo or ligand-bound RORγt crystals were obtained with 2–8% (w/v) PEG4000, 0.6 M NaCl, and 0.1 M PIPES, pH 7.0. Crystals were flash-frozen in liquid nitrogen with cryoprotectant prepared using the corresponding reservoir condition supplemented with 20% glycerol. Protein–ligand co-crystals were obtained either from soaking

of the compound into apo RORγt crystals or from co-crystallization of the pre-formed protein–ligand complex solution. For co-crystallization, a compound was added to the protein stock solution with a protein–ligand molar ratio of about 1:5. The complex solution was incubated at room temperature for 40 min and then centrifuged at 14,000 rpm for 35 min prior to crystallization experiments. For soaking experiments, 3 mM compound prepared in DMSO stock solution was added in a drop containing the apo RORγt crystals and soaked at room temperature for 6 h. The soaked crystals were then flash-frozen in liquid nitrogen using the crystallization solution supplemented with 25% PEG400 as a cryoprotectant. X-ray diffraction data were collected at beamlines X06SA or X06DA (for co-crystals with compound **1**) of the Swiss Light Source using Pilatus 6M and 2M-F detectors, respectively. Diffraction data were processed using either d*TREK or XDS (69, 70). The initial structure was determined by molecular replacement with Phaser (71) as implemented in the PHENIX software suite (72) using the structure of RORγt LBD in complex with 22(*R*)-hydroxycholesterol (PDB code 3L0J) as a search model. Ligand geometry restraints were generated using Corina (Molecular Networks GmbH). Multiple rounds of positional and isotropic B-factor refinement using phenix.refine followed by manual rebuilding using Coot (73) were carried out for each structure. The quality of the final model was evaluated using MolProbity (74). Structural figures were generated using PyMOL (Schrödinger, LLC).

### NMR spectroscopy

All NMR data were acquired at 30 °C on an 800-MHz Bruker AvanceIII spectrometer equipped with a triple resonance ($^1$H/$^{13}$C/$^{15}$N) cryoprobe. 0.22 mM samples of uniformly $^{13}$C/$^{15}$N-labeled RORγt(259–518) or RORγt(260–507)-G$_3$-SRC2 in the same buffer containing 25 mM deuterated HEPES, pH 7.0, 150 mM NaCl, 2 mM DTT, with 10% D$_2$O, 90% H$_2$O were used in the NMR experiments. Each NMR sample had a volume of 140 $\mu$l using 2.5-mm Bruker Match tubes. For the titration experiments, SRC2 peptide was added to the RORγt(259–518) sample with a final total peptide concentration of 0.4 mM. The $^{15}$N-TROSY and $^{13}$C-HSQC experiments were carried out as described in the literature (75–77).

### Fluorescence polarization competitive binding assays

The fluorescence polarization (FP) measurements were conducted using an Envision plate reader (PerkinElmer Life Sciences) using the RORγt-SRC2 construct produced in-house (see above), and a fluorescent TAMRA (Thermo Fisher Scientific, Inc.) probe synthesized with an in-house compound binding to RORγt. Compound was diluted in assay buffer (20 mM Tris, pH 7.5, 150 mM NaCl, and 0.05% CHAPS), and 10 $\mu$l of 20 $\mu$M compound was mixed with 10 $\mu$l of 2 $\mu$M RORγt-SRC2 in the same buffer and incubated for 30 min at room temperature. The TAMRA probe was then added to the mixture at a final concentration of 15 nM. After 30 min of incubation at room temperature, the FP signal was measured (excitation wavelength 531 nm; emission wavelength 595 nm), and the $K_d$ values were determined as described (78).

### RORγt-Gal4 reporter gene assay

HEK293T cells were co-transfected with a plasmid pBIND containing the chimera of the DNA-binding domain of the yeast Gal4 protein and the ligand-binding domain of human RORγt (Gal4DBD-hRORγt LBD), along with the luciferase reporter plasmid pGL4.31 (luc2P/GAL4UAS/Hygro, Promega). The positive control was co-transiently transfected with both plasmids, and the negative control had only the pGL4.31 promoter sequence. Assays were assembled in 384-well Greiner plates where transiently transfected cells and test compound at varying concentrations were incubated at 37 °C and 5% CO$_2$ for 20–24 h. The next day, assay plates were taken out and equilibrated at room temperature for 20–30 min. Bright-Glo$^{TM}$ luciferase assay system (Promega) was used to detect luciferase production. After addition of Bright-Glo detection reagent, the plates were incubated at room temperature for 20 min. The plates were read on an Envision plate reader to measure luminescence signal. The relative light unit (RLU) signal was converted to percent of control value relative to control and blank wells.

### IL-17 production in Th17 primary cell assay

Frozen CD4$^+$ T cells (AllCells) were thawed and resuspended in X-VIVO media (Lonza) at a cell density of $1 \times 10^6$ cells/ml. Skewing cytokines were added to media at the final concentrations of 30 ng/ml IL-23, 10 ng/ml IL-1$\beta$, 10 ng/ml IL-6, 2 ng/ml IL-2, 4 ng/ml TGF$\beta$1, 5 $\mu$g/ml IL-4, and 5 $\mu$g/ml IFN$\gamma$ and mixed with activated beads (Miltenyi Biotec catalogue no. 130-091-441) at 1 bead/cell. The cells were incubated under the stimulatory conditions for 72 h at 37 °C. Skewed cells were spun and resuspended in Iscove's media (Invitrogen catalogue no. 12440) with a cell density of $1.11 \times 10^6$ cells/ml. Cells were seeded at 90 $\mu$l/well into Corning black/clear TC-treated plates (Corning catalogue no. 3603) to give 100,000 cells per well. 10 $\mu$l of medium-diluted compounds was added, and plates were incubated for 2 h at 37 °C and 5% CO$_2$. 50 $\mu$l of cytokine/bead mixture was added to all wells except blank wells, which received media only. Cell plates were incubated at 37 °C and 5% CO$_2$ for 48 h. Afterward, plates were spun, and 50 $\mu$l of supernatant from each well was collected and transferred to MSD Vplex IL-17A assay plate (Meso Scale Diagnostics, LLC) for detection of IL-17 expression, following the manufacturer's protocol. IC$_{50}$ values were obtained by fitting 10-point concentration-response data to a four-parameter logistic equation in ActivityBase (ID Business Solutions Ltd.).

### Coactivator recruitment assay

An FP-based assay was developed for coactivator recruitment. The fluorescence polarization measurements were conducted on an Envision (PerkinElmer Life Sciences) using a RORγt-GST construct produced in-house. The probe is a fluorescein-labeled coactivator peptide (D22) from Invitrogen containing the L*XX*LL motif and optimized for binding to RORγt ligand-binding domain. 10 $\mu$l of compounds diluted in 20 mM Tris, pH 7.5, 150 mM NaCl, and 0.05% CHAPS were mixed to 10 $\mu$l of 2 $\mu$M RORγt-GST in the same buffer and incubated for 30 min at room temperature. The fluorescein D22 probe was then added to the mixture at a final concentration of 15 nM. After 30 min of incubation at room temperature, the FP signal was mea-

sured (excitation wavelength 480 nm; emission wavelength 535 nm).

## DFT calculation

Interaction energies between His-479, Tyr-502, and Phe-506 of RORγt LBD were calculated using the DFT routine implemented in Jaguar (79). A hybrid functional for non-covalent complexation energies, M06-2X (80), was applied together with a $6-31G^{**}$ basis set to calculate DFT energies. A self-consistent reaction field method using a Poisson Boltzmann solver (81) was applied as continuum solvation model with a dielectric constant of $\epsilon = 4$. Interaction energies were calculated as the difference between the DFT energy of the residue triplet with atomic coordinates of His-479, Tyr-502, and Phe-506 taken from the crystal structures reported here and three DFT energies associated with the individual residues calculated separately. To preserve the coordinates found in the crystal structures, only single point energies were calculated. The interaction energies for corresponding PPARγ residues were calculated based on the same DFT method, with PPARγ coordinates taken from PDB code 1PRG.

---

## References

1. Korn, T., Bettelli, E., Oukka, M., and Kuchroo, V. K. (2009) IL-17 and Th17 cells. *Annu. Rev. Immunol.* **27,** 485–517
2. Glocker, E., and Grimbacher, B. (2010) Chronic mucocutaneous candidiasis and congenital susceptibility to *Candida. Curr. Opin. Allergy Clin. Immunol.* **10,** 542–550
3. Glocker, E. O., and Grimbacher, B. (2011) Mucosal antifungal defence: IL-17 signalling takes centre stage. *Immunol. Cell Biol.* **89,** 823–825
4. Langrish, C. L., Chen, Y., Blumenschein, W. M., Mattson, J., Basham, B., Sedgwick, J. D., McClanahan, T., Kastelein, R. A., and Cua, D. J. (2005) IL-23 drives a pathogenic T cell population that induces autoimmune inflammation. *J. Exp. Med.* **201,** 233–240
5. Cua, D. J., Sherlock, J., Chen, Y., Murphy, C. A., Joyce, B., Seymour, B., Lucian, L., To, W., Kwan, S., Churakova, T., Zurawski, S., Wiekowski, M., Lira, S. A., Gorman, D., Kastelein, R. A., and Sedgwick, J. D. (2003) Interleukin-23 rather than interleukin-12 is the critical cytokine for autoimmune inflammation of the brain. *Nature* **421,** 744–748
6. Lubberts, E., Koenders, M. I., Oppers-Walgreen, B., van den Bersselaar, L., Coenen-de Roo, C. J., Joosten, L. A., and van den Berg, W. B. (2004) Treatment with a neutralizing anti-murine interleukin-17 antibody after the onset of collagen-induced arthritis reduces joint inflammation, cartilage destruction, and bone erosion. *Arthritis Rheum.* **50,** 650–659
7. Sarkar, S., and Fox, D. A. (2010) Targeting IL-17 and Th17 cells in rheumatoid arthritis. *Rheum. Dis. Clin. North Am.* **36,** 345–366
8. Sherlock, J. P., Joyce-Shaikh, B., Turner, S. P., Chao, C. C., Sathe, M., Grein, J., Gorman, D. M., Bowman, E. P., McClanahan, T. K., Yearley, J. H., Eberl, G., Buckley, C. D., Kastelein, R. A., Pierce, R. H., Laface, D. M., and Cua, D. J. (2012) IL-23 induces spondyloarthropathy by acting on ROR-γt+ CD3+CD4-CD8− entheseal resident T cells. *Nat. Med.* **18,** 1069–1076
9. Duerr, R. H., Taylor, K. D., Brant, S. R., Rioux, J. D., Silverberg, M. S., Daly, M. J., Steinhart, A. H., Abraham, C., Regueiro, M., Griffiths, A., Dassopoulos, T., Bitton, A., Yang, H., Targan, S., Datta, L. W., *et al.* (2006) A genome-wide association study identifies IL23R as an inflammatory bowel disease gene. *Science* **314,** 1461–1463
10. Liu, Y., Helms, C., Liao, W., Zaba, L. C., Duan, S., Gardner, J., Wise, C., Miner, A., Malloy, M. J., Pullinger, C. R., Kane, J. P., Saccone, S., Worthington, J., Bruce, I., Kwok, P. Y., *et al.* (2008) A genome-wide association study of psoriasis and psoriatic arthritis identifies new disease loci. *PLoS Genet.* **4,** e1000041
11. Lock, C., Hermans, G., Pedotti, R., Brendolan, A., Schadt, E., Garren, H., Langer-Gould, A., Strober, S., Cannella, B., Allard, J., Klonowski, P., Austin, A., Lad, N., Kaminski, N., Galli, S. J., *et al.* (2002) Gene-microarray analysis of multiple sclerosis lesions yields new targets validated in autoimmune encephalomyelitis. *Nat. Med.* **8,** 500–508
12. Australo-Anglo-American Spondyloarthritis Consortium (TASC), Reveille, J. D., Sims, A. M., Danoy, P., Evans, D. M., Leo, P., Pointon, J. J., Jin, R., Zhou, X., Bradbury, L. A., Appleton, L. H., Davis, J. C., Diekman, L., Doan, T., Dowling, A., *et al.* (2010) Genome-wide association study of ankylosing spondylitis identifies non-MHC susceptibility loci. *Nat. Genet.* **42,** 123–127
13. Miossec, P., and Kolls, J. K. (2012) Targeting IL-17 and TH17 cells in chronic inflammation. *Nat. Rev. Drug Discov.* **11,** 763–776
14. Burkett, P. R., and Kuchroo, V. K. (2016) IL-17 blockade in psoriasis. *Cell* **167,** 1669
15. Patel, D. D., and Kuchroo, V. K. (2015) Th17 Cell pathway in human immunity: lessons from genetics and therapeutic interventions. *Immunity* **43,** 1040–1051
16. Attia, A., Abushouk, A. I., Ahmed, H., Gadelkarim, M., Elgebaly, A., Hassan, Z., Abdel-Daim, M. M., and Negida, A. (2017) Safety and efficacy of brodalumab for moderate-to-severe plaque psoriasis: a systematic review and meta-analysis. *Clin. Drug Investig.* **37,** 439–451
17. Ivanov, I. I., McKenzie, B. S., Zhou, L., Tadokoro, C. E., Lepelley, A., Lafaille, J. J., Cua, D. J., and Littman, D. R. (2006) The orphan nuclear receptor RORγt directs the differentiation program of proinflammatory IL-17+ T helper cells. *Cell* **126,** 1121–1133
18. Manel, N., Unutmaz, D., and Littman, D. R. (2008) The differentiation of human T(H)-17 cells requires transforming growth factor-β and induction of the nuclear receptor RORγt. *Nat. Immunol.* **9,** 641–649
19. Gaffen, S. L., Jain, R., Garg, A. V., and Cua, D. J. (2014) The IL-23–IL-17 immune axis: from mechanisms to therapeutic testing. *Nat. Rev. Immunol.* **14,** 585–600
20. Fauber, B. P., and Magnuson, S. (2014) Modulators of the nuclear receptor retinoic acid receptor-related orphan receptor-γ (RORγ or RORc). *J. Med. Chem.* **57,** 5871–5892
21. Cyr, P., Bronner, S. M., and Crawford, J. J. (2016) Recent progress on nuclear receptor RORγ modulators. *Bioorg. Med. Chem. Lett.* **26,** 4387–4393
22. Bronner, S. M., Zbieg, J. R., and Crawford, J. J. (2017) RORγ antagonists and inverse agonists: a patent review. *Expert Opin. Ther. Pat.* **27,** 101–112
23. Jetten, A. M. (2009) Retinoid-related orphan receptors (RORs): critical roles in development, immunity, circadian rhythm, and cellular metabolism. *Nucl. Recept. Signal.* **7,** e003
24. Hu, X., Wang, Y., Hao, L. Y., Liu, X., Lesch, C. A., Sanchez, B. M., Wendling, J. M., Morgan, R. W., Aicher, T. D., Carter, L. L., Toogood, P. L., and Glick, G. D. (2015) Sterol metabolism controls T(H)17 differentiation by generating endogenous RORγ agonists. *Nat. Chem. Biol.* **11,** 141–147
25. Santori, F. R., Huang, P., van de Pavert, S. A., Douglass, E. F., Jr., Leaver, D. J., Haubrich, B. A., Keber, R., Lorbek, G., Konijn, T., Rosales, B. N., Rozman, D., Horvat, S., Rahier, A., Mebius, R. E., Rastinejad, F., *et al.*

(2015) Identification of natural RORγ ligands that regulate the development of lymphoid cells. *Cell Metab.* **21,** 286–297

26. Soroosh, P., Wu, J., Xue, X., Song, J., Sutton, S. W., Sablad, M., Yu, J., Nelen, M. I., Liu, X., Castro, G., Luna, R., Crawford, S., Banie, H., Dandridge, R. A., Deng, X., *et al.* (2014) Oxysterols are agonist ligands of RORγt and drive Th17 cell differentiation. *Proc. Natl. Acad. Sci. U.S.A.* **111,** 12163–12168

27. Wang, C., Yosef, N., Gaublomme, J., Wu, C., Lee, Y., Clish, C. B., Kaminski, J., Xiao, S., Meyer Zu Horste, G., Pawlak, M., Kishi, Y., Joller, N., Karwacz, K., Zhu, C., Ordovas-Montanes, M., *et al.* (2015) CD5L/AIM regulates lipid biosynthesis and restrains Th17 cell pathogenicity. *Cell* **163,** 1413–1427

28. Jin, L., Martynowski, D., Zheng, S., Wada, T., Xie, W., and Li, Y. (2010) Structural basis for hydroxycholesterols as natural ligands of orphan nuclear receptor RORγ. *Mol. Endocrinol.* **24,** 923–929

29. Fujita-Sato, S., Ito, S., Isobe, T., Ohyama, T., Wakabayashi, K., Morishita, K., Ando, O., and Isono, F. (2011) Structural basis of digoxin that antagonizes RORγt receptor activity and suppresses Th17 cell differentiation and interleukin (IL)-17 production. *J. Biol. Chem.* **286,** 31409–31417

30. Fauber, B. P., de Leon Boenig, G., Burton, B., Eidenschenk, C., Everett, C., Gobbi, A., Hymowitz, S. G., Johnson, A. R., Liimatta, M., Lockey, P., Norman, M., Ouyang, W., René, O., and Wong, H. (2013) Structure-based design of substituted hexafluoroisopropanol-arylsulfonamides as modulators of RORc. *Bioorg. Med. Chem. Lett.* **23,** 6604–6609

31. Muegge, I., Collin, D., Cook, B., Hill-Drzewi, M., Horan, J., Kugler, S., Labadia, M., Li, X., Smith, L., and Zhang, Y. (2015) Discovery of 1,3-dihydro-2,1,3-benzothiadiazole 2,2-dioxide analogs as new RORC modulators. *Bioorg. Med. Chem. Lett.* **25,** 1892–1895

32. Enyedy, I. J., Powell, N. A., Caravella, J., van Vloten, K., Chao, J., Banerjee, D., Marcotte, D., Silvian, L., McKenzie, A., Hong, V. S., and Fontenot, J. D. (2016) Discovery of biaryls as RORγ inverse agonists by using structure-based design. *Bioorg. Med. Chem. Lett.* **26,** 2459–2463

33. Hirata, K., Kotoku, M., Seki, N., Maeba, T., Maeda, K., Hirashima, S., Sakai, T., Obika, S., Hori, A., Hase, Y., Yamaguchi, T., Katsuda, Y., Hata, T., Miyagawa, N., Arita, K., *et al.* (2016) SAR exploration guided by LE and Fsp(3): discovery of a selective and orally efficacious RORγ inhibitor. *ACS Med. Chem. Lett.* **7,** 23–27

34. Marcotte, D. J., Liu, Y., Little, K., Jones, J. H., Powell, N. A., Wildes, C. P., Silvian, L. F., and Chodaparambil, J. V. (2016) Structural determinant for inducing RORγ specific inverse agonism triggered by a synthetic benzoxazinone ligand. *BMC Struct. Biol.* **16,** 7

35. René, O., Fauber, B. P., Boenig Gde, L., Burton, B., Eidenschenk, C., Everett, C., Gobbi, A., Hymowitz, S. G., Johnson, A. R., Kiefer, J. R., Liimatta, M., Lockey, P., Norman, M., Ouyang, W., Wallweber, H. A., and Wong, H. (2015) Minor structural change to tertiary sulfonamide RORc ligands led to opposite mechanisms of action. *ACS Med. Chem. Lett.* **6,** 276–281

36. Scheepstra, M., Leysen, S., van Almen, G. C., Miller, J. R., Piesvaux, J., Kutilek, V., van Eenennaam, H., Zhang, H., Barr, K., Nagpal, S., Soisson, S. M., Kornienko, M., Wiley, K., Elsen, N., Sharma, S., *et al.* (2015) Identification of an allosteric binding site for RORγt inhibition. *Nat. Commun.* **6,** 8833

37. Jencks, W. P. (1981) On the attribution and additivity of binding energies. *Proc. Natl. Acad. Sci. U.S.A.* **78,** 4046–4050

38. Knotts T. A., 4th, Rathore, N., and de Pablo, J. J. (2008) An entropic perspective of protein stability on surfaces. *Biophys. J.* **94,** 4473–4483

39. Wang, W., Prosise, W. W., Chen, J., Taremi, S. S., Le, H. V., Madison, V., Cui, X., Thomas, A., Cheng, K. C., and Lesburg, C. A. (2008) Construction and characterization of a fully active PXR/SRC-1 tethered protein with increased stability. *Protein Eng. Des. Sel.* **21,** 425–433

40. Fremont, D. H., Hendrickson, W. A., Marrack, P., and Kappler, J. (1996) Structures of an MHC class II molecule with covalently bound single peptides. *Science* **272,** 1001–1004

41. Reddy Chichili, V. P., Kumar, V., and Sivaraman, J. (2013) Linkers in the structural biology of protein-protein interactions. *Protein Sci.* **22,** 153–167

42. Hohenstein, E. G., Chill, S. T., and Sherrill, C. D. (2008) Assessment of the performance of the M05–2X and M06–2X exchange-correlation functionals for noncovalent interactions in biomolecules. *J. Chem. Theory Comput.* **4,** 1996–2000

43. Zhao, Y., and Truhlar, D. G. (2008) Density functionals with broad applicability in chemistry. *Acc. Chem. Res.* **41,** 157–167

44. Johnson, B. A., Wilson, E. M., Li, Y., Moller, D. E., Smith, R. G., and Zhou, G. (2000) Ligand-induced stabilization of PPARγ monitored by NMR spectroscopy: implications for nuclear receptor activation. *J. Mol. Biol.* **298,** 187–194

45. Kallenberger, B. C., Love, J. D., Chatterjee, V. K., and Schwabe, J. W. (2003) A dynamic mechanism of nuclear receptor activation and its perturbation in a human disease. *Nat. Struct. Biol.* **10,** 136–140

46. Nolte, R. T., Wisely, G. B., Westin, S., Cobb, J. E., Lambert, M. H., Kurokawa, R., Rosenfeld, M. G., Willson, T. M., Glass, C. K., and Milburn, M. V. (1998) Ligand binding and co-activator assembly of the peroxisome proliferator-activated receptor-γ. *Nature* **395,** 137–143

47. Eilers, M., Shekar, S. C., Shieh, T., Smith, S. O., and Fleming, P. J. (2000) Internal packing of helical membrane proteins. *Proc. Natl. Acad. Sci. U.S.A.* **97,** 5796–5801

48. Edwards, T. A., and Wilson, A. J. (2011) Helix-mediated protein–protein interactions as targets for intervention using foldamers. *Amino Acids* **41,** 743–754

49. Vihinen, M., Torkkila, E., and Riikonen, P. (1994) Accuracy of protein flexibility predictions. *Proteins* **19,** 141–149

50. Parthasarathy, S., and Murthy, M. R. (2000) Protein thermal stability: insights from atomic displacement parameters (B values). *Protein Eng.* **13,** 9–13

51. Yuan, Z., Zhao, J., and Wang, Z. X. (2003) Flexibility analysis of enzyme active sites by crystallographic temperature factors. *Protein Eng.* **16,** 109–114

52. Fenwick, R. B., van den Bedem, H., Fraser, J. S., and Wright, P. E. (2014) Integrated description of protein dynamics from room-temperature X-ray crystallography and NMR. *Proc. Natl. Acad. Sci. U.S.A.* **111,** E445–E454

53. Gustafsson, J. A. (2016) Historical overview of nuclear receptors. *J. Steroid Biochem. Mol. Biol.* **157,** 3–6

54. Renaud, J. P., and Moras, D. (2000) Structural studies on nuclear receptors. *Cell. Mol. Life Sci.* **57,** 1748–1769

55. Pardee, K. I., Xu, X., Reinking, J., Schuetz, A., Dong, A., Liu, S., Zhang, R., Tiefenbach, J., Lajoie, G., Plotnikov, A. N., Botchkarev, A., Krause, H. M., and Edwards, A. (2009) The structural basis of gas-responsive transcription by the human nuclear hormone receptor REV-ERBβ. *PLoS Biol.* **7,** e43

56. Raghuram, S., Stayrook, K. R., Huang, P., Rogers, P. M., Nosie, A. K., McClure, D. B., Burris, L. L., Khorasanizadeh, S., Burris, T. P., and Rastinejad, F. (2007) Identification of heme as the ligand for the orphan nuclear receptors REV-ERBα and REV-ERBβ. *Nat. Struct. Mol. Biol.* **14,** 1207–1213

57. Perissi, V., and Rosenfeld, M. G. (2005) Controlling nuclear receptors: the circular logic of cofactor cycles. *Nat. Rev. Mol. Cell Biol.* **6,** 542–554

58. Rastinejad, F., Ollendorff, V., and Polikarpov, I. (2015) Nuclear receptor full-length architectures: confronting myth and illusion with high resolution. *Trends Biochem. Sci.* **40,** 16–24

59. Rastinejad, F., Huang, P., Chandra, V., and Khorasanizadeh, S. (2013) Understanding nuclear receptor form and function using structural biology. *J. Mol. Endocrinol.* **51,** T1-T21

60. Anbalagan, M., Huderson, B., Murphy, L., and Rowan, B. G. (2012) Posttranslational modifications of nuclear receptors and human disease. *Nucl. Recept. Signal.* **10,** e001

61. Faus, H., and Haendler, B. (2006) Post-translational modifications of steroid receptors. *Biomed. Pharmacother.* **60,** 520–528

62. Lim, H. W., Kang, S. G., Ryu, J. K., Schilling, B., Fei, M., Lee, I. S., Kehasse, A., Shirakawa, K., Yokoyama, M., Schnölzer, M., Kasler, H. G., Kwon, H. S., Gibson, B. W., Sato, H., Akassoglou, K., *et al.* (2015) SIRT1 deacetylates RORγt and enhances Th17 cell generation. *J. Exp. Med.* **212,** 607–617

63. Rutz, S., Kayagaki, N., Phung, Q. T., Eidenschenk, C., Noubade, R., Wang, X., Lesch, J., Lu, R., Newton, K., Huang, O. W., Cochran, A. G., Vasser, M., Fauber, B. P., DeVoss, J., Webster, J., *et al.* (2015) Deubiquitinase DUBA is a post-translational brake on interleukin-17 production in T cells. *Nature* **518,** 417–421

64. Gallastegui, N., Mackinnon, J. A., Fletterick, R. J., and Estébanez-Perpiñá, E. (2015) Advances in our structural understanding of orphan nuclear receptors. *Trends Biochem. Sci.* **40,** 25–35

65. Sablin, E. P., Krylova, I. N., Fletterick, R. J., and Ingraham, H. A. (2003) Structural basis for ligand-independent activation of the orphan nuclear receptor LRH-1. *Mol. Cell* **11,** 1575–1585

66. Fujioka, M., and Omori, N. (2012) Subtleties in GPCR drug discovery: a medicinal chemistry perspective. *Drug Discov. Today* **17,** 1133–1138

67. Manglik, A., Kim, T. H., Masureel, M., Altenbach, C., Yang, Z., Hilger, D., Lerch, M. T., Kobilka, T. S., Thian, F. S., Hubbell, W. L., Prosser, R. S., and Kobilka, B. K. (2015) Structural insights into the dynamic process of β2-adrenergic receptor signaling. *Cell* **161,** 1101–1111

68. Staus, D. P., Strachan, R. T., Manglik, A., Pani, B., Kahsai, A. W., Kim, T. H., Wingler, L. M., Ahn, S., Chatterjee, A., Masoudi, A., Kruse, A. C., Pardon, E., Steyaert, J., Weis, W. I., Prosser, R. S., *et al.* (2016) Allosteric nanobodies reveal the dynamic range and diverse mechanisms of G-protein-coupled receptor activation. *Nature* **535,** 448–452

69. Pflugrath, J. W. (1999) The finer things in X-ray diffraction data collection. *Acta Crystallogr. D Biol. Crystallogr.* **55,** 1718–1725

70. Kabsch, W. (2010) XDS. *Acta Crystallogr. D Biol. Crystallogr.* **66,** 125–132

71. McCoy, A. J., Grosse-Kunstleve, R. W., Adams, P. D., Winn, M. D., Storoni, L. C., and Read, R. J. (2007) Phaser crystallographic software. *J. Appl. Crystallogr.* **40,** 658–674

72. Adams, P. D., Afonine, P. V., Bunkóczi, G., Chen, V. B., Davis, I. W., Echols, N., Headd, J. J., Hung, L. W., Kapral, G. J., Grosse-Kunstleve, R. W., McCoy, A. J., Moriarty, N. W., Oeffner, R., Read, R. J., Richardson, D. C., *et al.* (2010) PHENIX: a comprehensive Python-based system for macromolecular structure solution. *Acta Crystallogr. D Biol. Crystallogr.* **66,** 213–221

73. Emsley, P., and Cowtan, K. (2004) Coot: model-building tools for molecular graphics. *Acta Crystallogr. D Biol. Crystallogr.* **60,** 2126–2132

74. Chen, V. B., Arendall, W. B., 3rd, Headd, J. J., Keedy, D. A., Immormino, R. M., Kapral, G. J., Murray, L. W., Richardson, J. S., and Richardson, D. C. (2010) MolProbity: all-atom structure validation for macromolecular crystallography. *Acta Crystallogr. D Biol. Crystallogr.* **66,** 12–21

75. Nietlispach, D. (2005) Suppression of anti-TROSY lines in a sensitivity enhanced gradient selection TROSY scheme. *J. Biomol. NMR* **31,** 161–166

76. Hwang, T. L., van Zijl, P. C., and Garwood, M. (1997) Broadband adiabatic refocusing without phase distortion. *J. Magn. Reson.* **124,** 250–254

77. Kupce, E., and Freeman, R. (2007) Compensated adiabatic inversion pulses: broadband INEPT and HSQC. *J. Magn. Reson.* **187,** 258–265

78. Kashem, M. A., Nelson, R. M., Yingling, J. D., Pullen, S. S., Prokopowicz, A. S., 3rd, Jones, J. W., Wolak, J. P., Rogers, G. R., Morelock, M. M., Snow, R. J., Homon, C. A., and Jakes, S. (2007) Three mechanistically distinct kinase assays compared: measurement of intrinsic ATPase activity identified the most comprehensive set of ITK inhibitors. *J. Biomol. Screen* **12,** 70–83

79. Bochevarov, A. D., Harder, E., Hughes, T. F., Greenwood, J. R., Braden, D. A., Philipp, D. M., Rinaldo, D., Halls, M. D., Zhang, J., and Friesner, R. A. (2013) Jaguar: A high-performance quantum chemistry software program with strengths in life and materials sciences. *Int. J. Quantum Chem.* **113,** 2110–2142

80. Zhao, Y., and Truhlar, D. G. (2006) A new local density functional for main-group thermochemistry, transition metal bonding, thermochemical kinetics, and noncovalent interactions. *J. Chem. Phys.* **125,** 194101

81. Tannor, D. J., Marten, B., Murphy, R., Friesner, R. A., Sitkoff, D., Nicholls, A., Honig, B., Ringnalda, M., and Goddard, W. A. (1994) Accurate first principles calculation of molecular charge distributions and solvation energies from Ab initio quantum mechanics and continuum dielectric theory. *J. Am. Chem. Soc.* **116,** 11875–11882